canonical pathway makes it possible to identify the canonical pathway showing the most significant contribution to the extracted network. The significance in the similarity between both is scored following the formula, where O = the number of overlapping molecular relations between the extracted network and the canonical pathway, V = the number of molecular relations located in the extracted network, C = the number of molecular relations located in the canonical pathway, T = the number of total molecular relations, and the X = the sigma variable that defines coincidence.

$$\text{Score} = -\log_2(\text{Score(p)}) \quad \text{Score (p)} = \sum_{x=O}^{Min(C,V)} f(x)$$

$$f(x) = {}_{C}C_{x} \cdot {}_{T-C}C_{V-x} / {}_{T}C_{V}$$

Transient Expression of SREBP2

To transiently overexpress sterol regulatory element-binding protein-2 (SREBP2), the gene encoding the N-terminal fragment of SREBP2 spanning amino acid residues 1–484 was amplified by PCR using PfuTurbo DNA polymerase (Stratagene, La Jolla, CA) and a sense and antisense primer set of 5′gcgatggacgacagcggcgagctg3′ and 5′tcacagaagaatccg tgagcggtc3′, and cloned in the expression vector pEF6 (Invitrogen). The vector was transfected into HMO6 cells by X-tremeGENE HP DNA transfection reagent (Roche Diagnostics). At 24 h after transfection, the cells were processed for western blot analysis. For the control, V5-tagged LacZ cloned in the pEF6 vector was transfected into sister cultures.

Western Blot Analysis

To prepare total protein extract, the cells were homogenized in RIPA buffer supplemented with a cocktail of protease inhibitors (Sigma). The protein extract was centrifuged at 12,000 rpm for 5 min at room temperature (RT). The protein concentration was determined by a Bradford assay kit (BioRad Hercules, CA, USA). The mixture of the supernatant and a 2× Lammeli loading buffer was boiled and separated on SDS-PAGE gels ranging from 8 to 12%. After gel electrophoresis, the protein was transferred onto nitrocellulose membranes, and immunolabeled at RT overnight with rabbit anti-poly-ADP-ribose-polymerase (PARP) antibody (#11835238001; Roche Diagnostics), rabbit anti-cleaved caspase-3 (Asp175) antibody (#9661; Cell Signaling Technology, Danvers, MA, USA), mouse anti-caspase-7 antibody (#9494; Cell Signaling Technology), rabbit anti-caspase-9 antibody (#9502; Cell Signaling Technology), rabbit anti-S1P1 antibody (sc-25489, EDG-1, H-60; Santa Cruz Biotechnology, Santa Cruz, CA), or goat anti-SREBP2 antibody (sc-8151, N-19; Santa Cruz Biotechnology). Then, the membranes were incubated at RT for 60 min with HRP-conjugated anti-mouse IgG, anti-rabbit IgG, or anti-goat IgG (Santa Cruz Biotechnology). The specific reaction was visualized by exposing the membranes to a chemiluminescent substrate (Thermo Scientific, Rockford, IL, USA).

In some experiments, the antibodies were stripped by incubating the membranes at 50°C for 30 min in stripping buffer, composed of 62.5 mM Tris-HCl, pH 6.7, 2% SDS, and 100 mM 2-mercaptoethanol. Then, the membranes were processed for relabeling with goat anti-heat shock protein HSP60 antibody (sc-1052, N-20; Santa Cruz Biotechnology) used for an internal control of protein loading, followed by incubation with HRP-conjugated anti-goat IgG.

Results

S1P Receptor Expression on Human Microglia Cell Line HMO6

The expression of five S1P receptor mRNAs in a panel of human neural cells and tissues was determined by RT-PCR. All the cells and tissues examined, including the human cerebrum (CBR), fetal astrocytes (AS), neuronal progenitor (NP) cells, NTera2 teratocarcinoma-derived neurons, SK-N-SH neuroblastoma, IMR-32 neuroblastoma, U-373MG astroglioma, and the microglia cell line HMO6, expressed varying levels of S1P1, S1P2, and S1P3 mRNAs, except for Y79 retinoblastoma that did not express S1P1 (Fig. 1a–c, lanes 2–10). In contrast, the levels of G3PDH, a housekeeping gene, were almost constant in the cells and tissues examined (Fig. 1f, lanes 2–10). Although discernible levels of S1P4 and S1P5 mRNAs were identified in the human cerebrum (CBR), both of these mRNAs were almost undetectable in HMO6 (Fig. 1d, e, lanes 2 and 10). No products were amplified when the reverse transcription step is omitted (Fig. 1a–f, lane 1). We verified S1P1 protein expression in HMO6 by western blot (not shown).

Non-Phosphorylated FTY720 Induced Apoptosis of HMO6

A 6 h-exposure of non-phosphorylated FTY720 (FTY720-non-P) induced LDH release from HMO6 cells and cell death in a dose-dependent manner with IC50 of 10.6 ± 2.0 μM (Fig. 2a, c). It is worthy to note that the concentration of FTY720-non-P at lower than 5 μM was completely ineffective in inducing cell death of HMO6 (Fig. 2a). Generally, LDH release did not discriminate apoptotic and necrotic cell death. The exposure of FTY720-non-P at a concentration of 10 μM mediated the cleavage of PARP in the incubation time longer than 4 h,

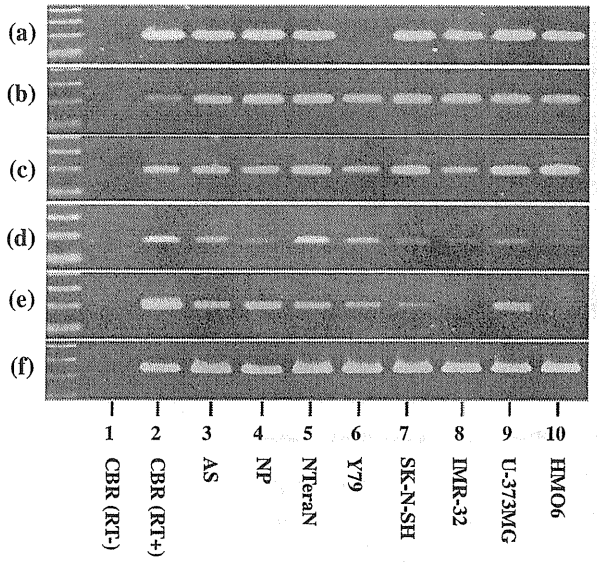

Fig. 1 S1P receptor expression in human neural cell lines. The expression of five S1P receptor mRNAs was studied by RT-PCR. **a** S1P1, **b** S1P2, **c** S1P3, **d** S1P4, **e** S1P5, and **f** G3PDH. The lanes (*1–10*) represent (*1*) the human frontal cerebral cortex (CBR) without inclusion of the reverse transcription (RT) step, (*2*) CBR with inclusion of the RT step, (*3*) cultured astrocytes (AS), (*4*) cultured neuronal progenitor (NP) cells, (*5*) NTera2 teratocarcinoma-derived neurons (NTera2N), (*6*) Y79 retinoblastoma, (*7*) SK-N-SH neuroblastoma, (*8*) IMR-32 neuroblastoma, (*9*) U-373MG astrocytoma, and (*10*) HMO6 microglia. The 100 bp ladder marker is shown on the left

indicating that FTY720-non-P induced cell death of HMO6 via apoptosis (Fig. 2d, lanes 7–10).

FTY720-non-P-induced apoptosis of HMO6 was accompanied by the cleavage of caspase-7 and caspase-3 (Fig. 3b, c, lane 2) but not of caspase-9 (Fig. 3e, lane 4), suggesting that the mitochondrial pathway of apoptosis that usually activates caspase-9 did not play a major role. Furthermore, Z-DQMD-FMK, a caspase-3-specific inhibitor, completely blocked FTY720-non-P-induced apoptosis of HMO6 (Fig. 3g, h, lane 10).

FTY720-Induced Apoptosis of HMO6 was Independent of S1P Receptor Binding

Because FTY720, when phosphorylated, binds to S1P1, S1P3, S1P4, and S1P5, all of which are G protein-coupled receptors (GPCR), we utilized Pertussis toxin (PTX), a Gi protein inhibitor, suramin, a S1P3/S1P5 inhibitor, and W123, a S1P1 competitive antagonist to block the ligand-receptor interaction. However, none of these receptor blockers could inhibit FTY720-induced apoptosis of HMO6 (Fig. 4a, lanes 4, 6, 8). Furthermore, SEW2871, a S1P1 selective agonist, and phosphorylated FTY720 (FTY720-P) at a concentration of 10 μM each did not induce apoptosis of HMO6 during the incubation time of 12 h (Fig. 4c, lanes 11 and 12). In addition, the combined administration of FTY720-P (10 μM) and FTY720-non-P (10 μM) did not inhibit apoptosis of HMO6, and treatment with sphiongosine-1 phosphate (S1P) (10–50 μM) did not induce apoptosis of HMO6 (data not shown). These results suggest that FTY720-non-P-induced apoptosis of HMO6 was independent of S1P receptor binding, and both FTY720-P and S1P were incapable of inducing apoptosis of HMO6.

FTY720 Induced SREBP-Responsive Genes

To investigate the molecular mechanism responsible for triggering FTY720-non-P-induced apoptosis of HMO6, we studied the genome-wide gene expression profile by microarray analysis. We identified 30 genes with an over 2-fold increase in HMO6 cells treated for 2 h with 10 μM FTY720-non-P versus those exposed to the vehicle (DMSO) (Table 1). Among them, the DAVID program categorized seven genes as a group of the genes associated with steroid and/or sterol metabolism (Table 1). None of apoptosis initiator and executor genes were induced in HMO6 cells at 2 h after initiation of the treatment. Upregulated expression of INSIG1 and LDLR in FTY720-non-P-treated HMO6 cells was validated by qPCR analysis (Fig. 5a, b).

Next, we imported the list of Entrez Gene IDs of the 30 genes upregulated in FTY720-non-P-treated HMO6 cells into KeyMolnet, a tool for analyzing molecular interactions on the comprehensive knowledgebase. KeyMolnet generated the molecular network, presenting with the most significant relationship with transcriptional regulation by sterol regulatory element-binding protein (SREBP) (the score = 69.719 with the *P*-value = 1.029E−21) (Fig. 5c). These results suggest that in HMO6 cells, FTY720-non-P activates SREBP proteins, either SREBP1 or SREBP2, belonging to the bHLH-Zip transcription factor family that promotes the synthesis of enzymes involved in cholesterol and fatty acid biosynthesis. To exclude a direct effect of vehicle (DMSO), in which FTY720-non-P was dissolved, on gene expression, we performed an additional set of microarray experiment by exposing HMO6 cells to FTY720-non-P dissolved in ethanol. We again identified the similar gene expression profile composed of upregulation of key SREBP-target genes, regardless of the solvent (See Table 1 in Electronic Supplementary Material).

SREBP2 is primarily involved in cholesterol synthesis, while SREBP1 chiefly regulates fatty acid synthesis (Sato 2010). INSIG1 identified by microarray analysis encodes an ER protein that plays a pivotal role in regulating intracellular cholesterol levels by interacting with SREBP cleavage-activating protein (SCAP) having the sterol-sensing domain activated by reduced cellular cholesterol levels. Thereafter, we have focused on SREBP2 expression

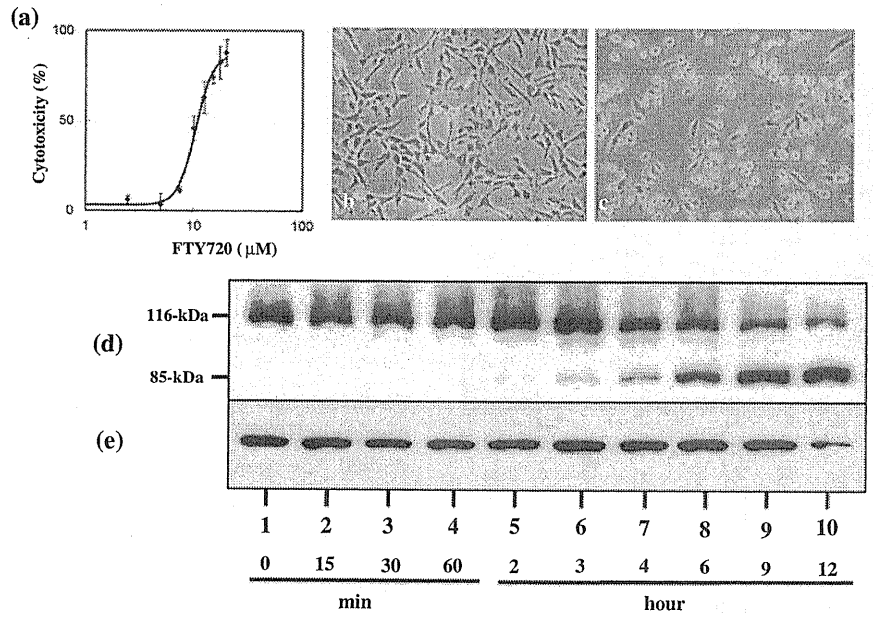

Fig. 2 Non-phosphorylated FTY720 induced apoptosis of HMO6 cells. HMO6 cells were exposed for various time periods to varying concentrations of non-phosphorylated FTY720 (FTY720-non-P). **a** LDH release assay, **b** the phase contrast photomicrograph of the cells exposed for 6 h to vehicle (DMSO), **c** the phase contrast photomicrograph of the cells exposed for 6 h to 10 μM FTY720-non-P, **d** western blot of PARP (an 116-kDa uncleaved form and an 85-kDa cleaved form), and **e** western blot of HSP60, an internal control of protein loading. The lanes (*1–10*) represent (*1*) untreated HMO6 cells, and HMO6 cells treated for (*2*) 15 min, (*3*) 30 min, (*4*) 1 h, (*5*) 2 h, (*6*) 3 h, (*7*) 4 h, (*8*) 6 h, (*9*) 9 h, and (*10*) 12 h with 10 μM FTY720-non-P

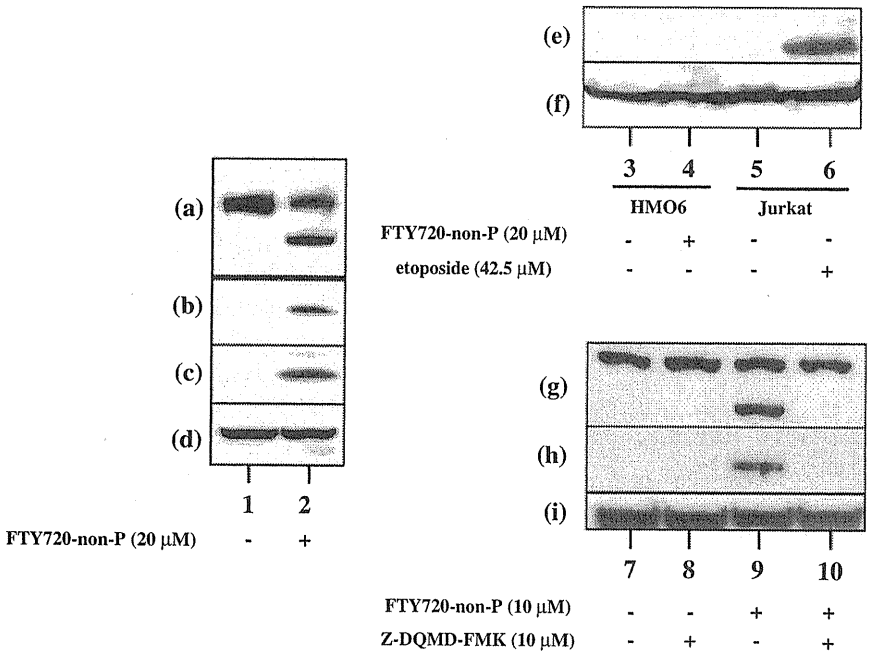

Fig. 3 FTY720-induced apoptosis of HMO6 was accompanied by activation of caspases 3 and 7. HMO6 cells were exposed for various time periods to varying concentrations of FTY720-non-P. For the positive control of caspase-9 activation, Jurkat cells were exposed to etoposide, an apoptosis-inducing agent. **a–i** indicate western blot of **a**, **g** PARP, **b** caspase-7 (a 20-kDa cleaved form), **c**, **h** caspase-3 (a 19-kDa cleaved form), **e** caspase-9 (a 37-kDa cleaved form), and **d**, **f**, **i** HSP60, an internal control of protein loading. The lanes (*1–10*) indicate HMO6 cells treated with (*1*, *3*) vehicle (DMSO) and (*2*, *4*) 20 μM FTY720-non-P for 9 h, and Jurkat cells treated with (*5*) vehicle (DMSO) and (*6*) 42.5 μM etoposide for 6 h, and (*7*) untreated HMO6 cells, and HMO6 cells treated with (*8*) 10 μM Z-DQMD-FMK, (*9*) 10 μM FTY720-non-P, and (*10*) a combination of 10 μM Z-DQMD-FMK and 10 μM FTY720-non-P for 12 h

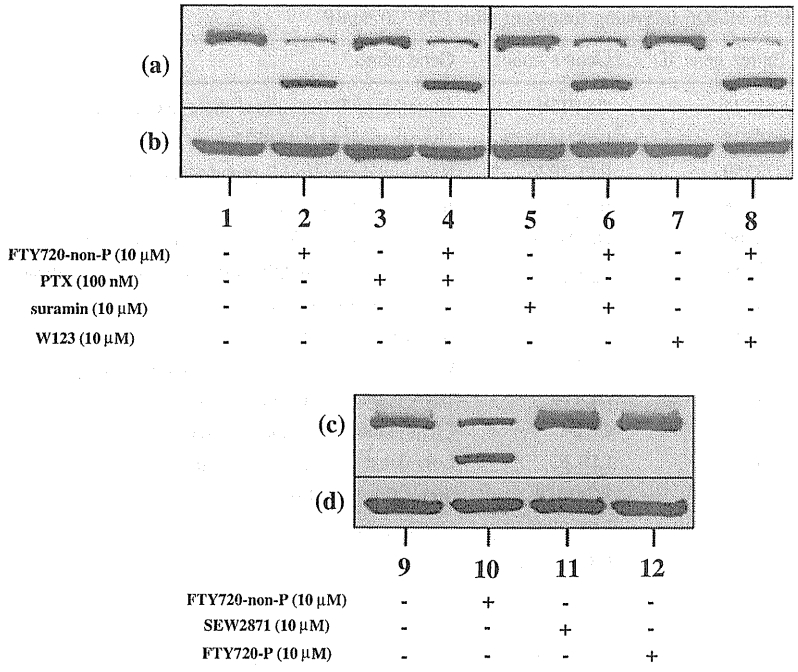

Fig. 4 FTY720-induced apoptosis of HMO6 was independent of S1P receptor binding. HMO6 cells were exposed for 12 h to 10 μM FTY720-non-P with or without inclusion of various S1P receptor agonists and antagonists. Pretreatment started at 30 min before exposure to FTY720-non-P. **a–d** indicate western blot of **a**, **c** PARP and **b**, **d** HSP60, an internal control of protein loading. The lanes (*1–12*) indicate (*1*, *9*) untreated HMO6 cells, and HMO6 cells treated with (*2*, *10*) 10 μM FTY720-non-P exposure alone, (*3*) 100 nM pertussis toxin (PTX) pretreatment alone, (4) 100 nM PTX pretreatment and 10 μM FTY720-non-P exposure, (*5*) 10 μM suramin pretreatment alone, (*6*) 10 μM suramin pretreatment and 10 μM FTY720-non-P exposure, (*7*) 10 μM W123 pretreatment alone, (*8*) 10 μM W123 pretreatment and 10 μM FTY720-non-P exposure, and HOM6 cells treated with a 12 h-exposure to (*11*) 10 μM SEW2871 or (*12*) 10 μM phosphorylated FTY720 (FTY720-P)

in HMO6 cells. The N-terminal fragment of SREBP2 is cleaved, dimerized, and translocated to the nucleus in response to the activating stimuli (Sato 2010). We identified the cleaved form of SREBP2 in HMO6 cells following an 1 h-exposure to FTY720-non-P ranging from 10 to 20 μM or by treatment with 3 μM simvastatin, a HMG-CoA reductase inhibitor capable of activating SREBP2 (Fig. 6a, lanes 2–4). Neither FTY720-non-P nor simvastatin alone at a concentration of 5 μM each induced apoptosis of HMO6 (Fig. 2a; Fig. 6b, lanes 7, 8). In contrast, a 12 h-pretreatment with 5 μM simvastatin enhanced FTY720-non-P-induced apoptosis of HMO6 cells, suggesting a proapoptotic effect mediated by SREBP2 activation following simvastatin treatment (Fig. 6b, lane 10).

A recent study showed that statins activate SREBP2, which positively controls the expression of caspase-7, resulting in induction of apoptosis of human gastric cancer cells (Gibot et al. 2009). When the N-terminal fragment of SREBP2 was overexpressed in HMO6 cells, the cleavage of PARP and caspase-3 was greatly enhanced, compared with the cells with overexpression of LacZ (Fig. 6c, f, lane 12), while the levels of procaspase-7 and cleaved caspase-7 were unaltered (Fig. 6g, lane 12).

Discussion

The present study revealed that non-phosphorylated FTY720 (FTY720-non-P) induced apoptosis of human microglia HM06 in a time- and dose-dependent manner with IC50 of 10.6 ± 2.0 μM. The apoptosis was inhibited by Z-DQMD-FMK, a caspase-3 inhibitor, but not by Pertussis toxin, a Gi protein inhibitor, suramin, a S1P3/S1P5 inhibitor, or W123, a S1P1 competitive antagonist, although HMO6 expressed S1P1, S1P2, and S1P3. Furthermore, both phosphorylated FTY720 (FTY720-P) and SEW2871, S1P1 selective agonists, did not induce apoptosis of HMO6. These observations suggest that FTY720-non-P-induced apoptosis of HMO6 cells is independent of S1P receptor binding.

Supporting these observations, FTY720, serving as a potential anti-cancer agent, induces apoptosis of various human cancer cell lines derived from liver, kidney, pancreas, and breast, multiple myeloma and leukemia cells, which is often mediated by S1P receptor-independent mechanisms (Matsuoka et al. 2003; Lee et al. 2004; Liu et al. 2010; Nagaoka et al. 2008). The concentrations required to induce apoptosis of tumor cells in vitro are about

Table 1 Upregulated genes in HMO6 following treatment with FTY720-non-P

Rank	Fold change	Entrez gene ID	Gene symbol	Gene name
1	5.75	25774	GSTTP1	Glutathione S-transferase theta pseudogene 1
2	3.16	150527	LOC150527	Hypothetical LOC150527
3	2.78	728380	RPL7P26	Ribosomal protein L7 pseudogene 26
4	2.74	3638	INSIG1	Insulin induced gene 1
5	2.72	158160	HSD17B7P2	Hydroxysteroid (17-beta) dehydrogenase 7 pseudogene 2
6	2.70	3157	HMGCS1	3-hydroxy-3-methylglutaryl-coenzyme A synthase 1 (soluble)
7	2.68	346007	EYS	Eyes shut homolog (Drosophila)
8	2.48	26834	RNU4-2	RNA, U4 small nuclear 2
9	2.46	163720	CYP4Z2P	Cytochrome P450, family 4, subfamily Z, polypeptide 2 pseudogene
10	2.44	54541	DDIT4	DNA-damage-inducible transcript 4
11	2.41	6351	CCL4	Chemokine (C–C motif) ligand 4
12	2.39	3949	LDLR	Low density lipoprotein receptor
13	2.37	6307	SC4MOL	Sterol-C4-methyl oxidase-like
14	2.34	286359	LOC286359	Hypothetical LOC286359
15	2.30	391003	PRAMEF18	PRAME family member 18
16	2.29	23175	LPIN1	Lipin 1
17	2.25	54897	CASZ1	Castor zinc finger 1
18	2.16	3156	HMGCR	3-hydroxy-3-methylglutaryl-coenzyme A reductase
19	2.16	196335	OR56B4	Olfactory receptor, family 56, subfamily B, member 4
20	2.10	3283	HSD3B1	Hydroxy-delta-5-steroid dehydrogenase, 3 beta- and steroid delta-isomerase 1
21	2.09	8553	BHLHE40	Basic helix-loop-helix family, member e40
22	2.07	10517	FBXW10	F-box and WD repeat domain containing 10
23	2.06	256892	OR51F1	Olfactory receptor, family 51, subfamily F, member 1
24	2.05	4598	MVK	Mevalonate kinase
25	2.04	196074	METT5D1	Methyltransferase 5 domain containing 1
26	2.04	901	CCNG2	Cyclin G2
27	2.03	439927	C1orf180	Chromosome 1 open reading frame 180
28	2.01	10551	AGR2	Anterior gradient homolog 2 (Xenopus laevis)
29	2.01	91074	ANKRD30A	Ankyrin repeat domain 30A
30	2.00	1831	TSC22D3	TSC22 domain family, member 3

HMO6 cells were exposed to non-phosporylated FTY720 (10 μM) or vehicle (DMSO) for 2 h. The genome-wide transcriptome was studied on Human Gene 1.0 ST array. The genes with an over 2-fold increase in FTY720-non-P-treated HMO6 cells are listed. The genes associated with steroid and/or sterol metabolism annotated by the DAVID program are underlined

two orders of magnitude greater than the blood concentration in the clinical setting, i.e., 5.4 ng/ml in plasma (Brinkmann et al. 2001, 2010). FTY720 has a half-life of approximately 10 days in vivo, and is cleared predominantly by a metabolic pathway requiring cytochrome P450 4F2 (CYP4F2) (Jin et al. 2011). The enzymatic activity of CYP4F2 is inhibited by certain drugs like ketoconazole, and the gene encoding CYP4F2 has a variety of single nucleotide polymorphisms (SNPs) (www.ncbi.nlm.nih.gov/snp). Therefore, in poor metabolizers of FTY720 receiving a CYP4F2 inhibitor, if they exist, the blood concentration of FTY720 could increase up to the range of toxic levels.

FTY720-non-P goes through the plasma membrane without requirement of the receptor binding, and targets directly key intracellular enzymes involved in sphingolipid metabolism, such as sphingosine kinases, phospholipase A2, and S1P lyase (Bandhuvula et al. 2005). FTY720 also inhibits ceramide synthases, resulting in a decrease in cellular levels of ceramide, dihydroceramide, shingosine, and S1P, and an increase in dihydrosphingosine and dihydroshingosine-1-phosphate, all of which alter the endogenous balance between survival and apoptotic signals (Berdyshev et al. 2009). FTY720-non-P promotes phosphorylation of 14-3-3zeta on Ser58 that disrupts 14-3-3 dimer formation, resulting in releasing proapototic mediators (Woodcock et al. 2010). FTY720, phosphorylated by SPHK2 located inside the plasma membrane, is transported outside the cells via the S1P transporter named spinster

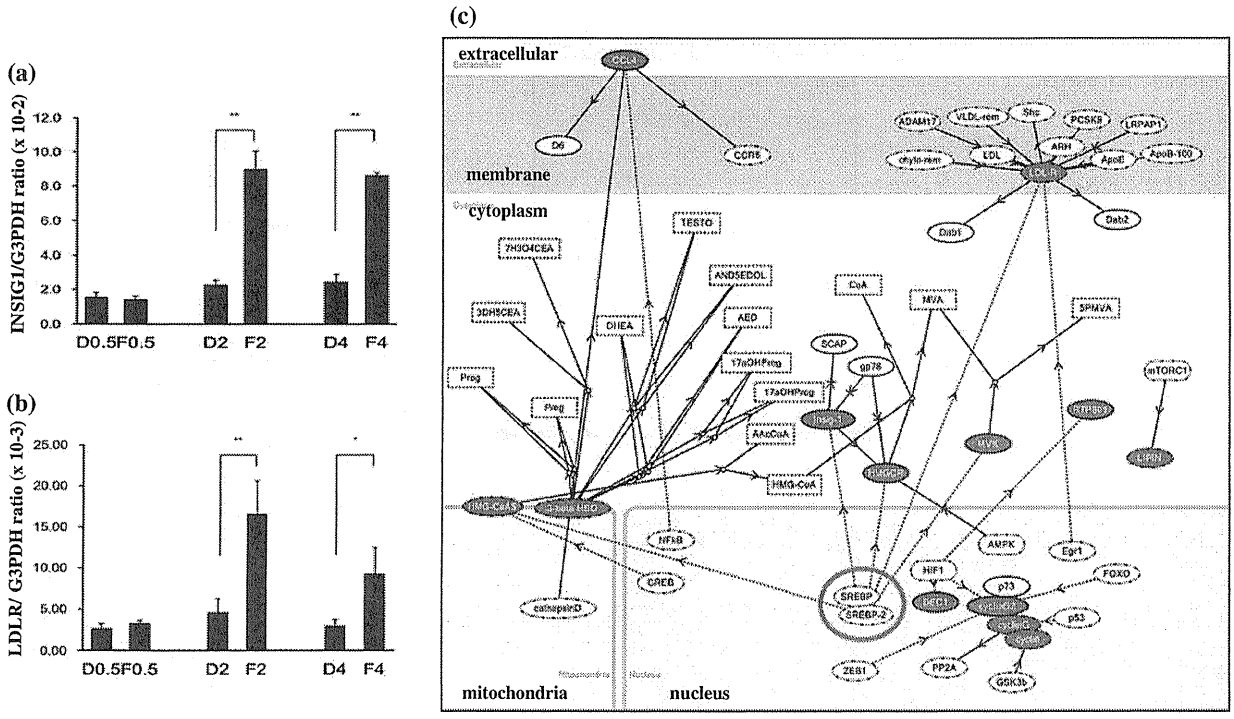

Fig. 5 FTY720 Induced SREBP-Responsive Genes. HMO6 cells were exposed for 2 h to 10 μM FTY720-non-P or vehicle (DMSO). Then, total RNA was processed for the genome-wide gene expression profiling on a microarray, followed by molecular network analysis by KeyMolnet and validation by qPCR. We identified 30 upregulated genes in FTY720-non-P-treated HMO6 cells (Table 1). **a–c** indicate qPCR of **a** INSIG1 and **b** LDLR, and **c** molecular network of FTY720-non-P-induced genes. Abbreviations: D, vehicle (DMSO); F, FTY720-non-P; 0.5, 30 min; 2, 2 h; and 4, 4 h. In **c**, red filled nodes represent FTY720-non-P-induced genes, whereas white open nodes exhibit additional nodes extracted automatically from the core contents of KeyMolnet to establish molecular connections. The molecular relation is indicated by solid line with arrow (direct binding or activation), solid line with arrow and stop (direct inactivation), solid line without arrow (complex formation), dash line with arrow (transcriptional activation), and dash line with arrow and stop (transcriptional repression). The transcription factor SREBP (SREBP2) is highlighted by a red thick circle

homolog 2 (SPNS2), and then the phosphorylated FTY720 binds to S1P receptors expressed on the surface of the plasma membrane (Hisano et al. 2011).

Being consistent with our observations, FTY720-non-P but not FTY720-P induces apoptosis of human breast and colon cancers (Nagaoka et al. 2008). FTY720 inhibits cytosolic phospholipase A2 ($cPLA_2$) in a manner independent of S1P receptor binding (Payne et al. 2007). FTY720-non-P but not FTY720-P inhibits PKC activation, which is associated with cell-surface expression of S1P1 (Sensken and Gräler 2010). Furthermore, FTY720-P counteracts FTY720-non-P-induced apoptosis of human fibroblasts by activating Bcl-2 (Potteck et al. 2010).

Several previous studies showed that FTY720-induced apoptosis is often accompanied by activation of a series of caspases (Wang et al. 1999). We found activation of both caspase-3 and caspase-7 during FTY720-non-P-induced apoptosis of HMO6. Furthermore, FTY720-induced apoptosis also involves various mechanisms, such as dephosphorylation of protein kinase B (Akt) (Matsuoka et al. 2003; Lee et al. 2004), deregulation of mitogen-activated protein kinases (MAPKs), focal adhesion kinase (FAK), and Rho-GTPase (Matsuda et al. 1999; Sonoda et al. 2001), and activation of protein phosphatase 2A (PP2A) (Liu et al. 2010). Here, we for the first time showed that FTY720-non-P-induced apoptosis of HMO6 cells is positively regulated by the SREBP2-dependent signaling pathway.

A recent study showed that statins induce apoptosis of human gastric cancer cells by activating SREBP1 and SREBP2, both of which transcriptionally upregulate caspase-7 (Gibot et al. 2009). Statin-dependent apoptosis is prevented by replenishment of mevalonate, the immediate product by the HMG-CoA reductase activity (Xia et al. 2001). A previous study showed that activation of caspase-3 releases SREBP proteins from ER membrane in a proteolytic reaction distinct from the sterol-regulated cleavage, resulting in nuclear transport of SREBP and transcriptional activation of sterol-regulatory genes (Higgins and Ioannou 2001). However, during FTY720-non-P-induced apoptosis of HMO6 cells, we identified activation of SREBP2 as early as at 1 h after initiation of the treatment, which is long before detection of the PARP cleavage, suggesting that

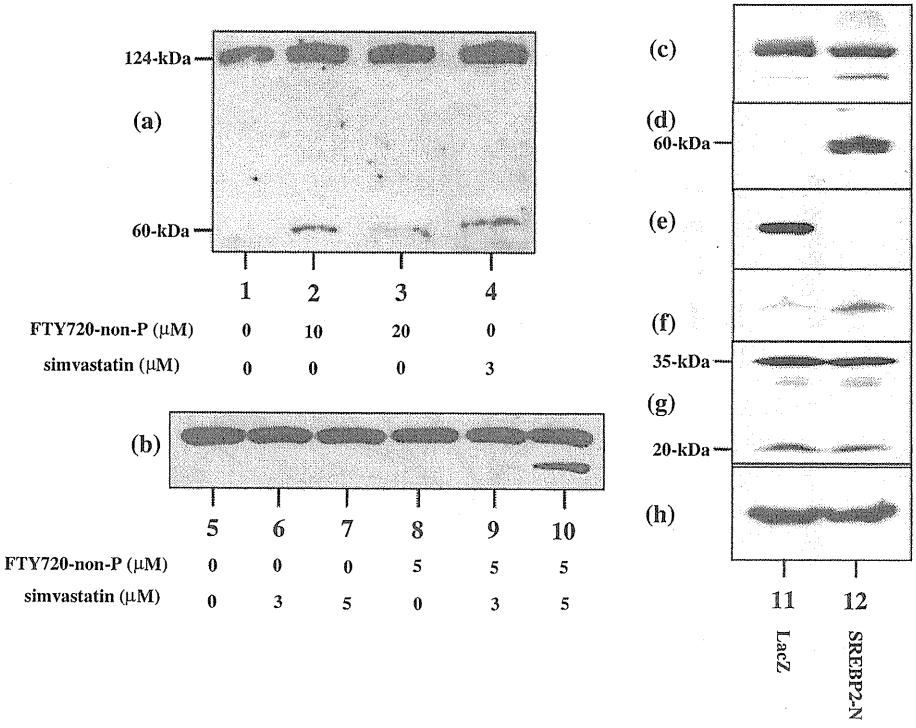

Fig. 6 Activation of SREBP2 by FTY720-non-P in HMO6 cells. HMO6 cells were exposed to FTY720-non-P or simvastatin, or transfected with the vector expressing the N-terminal fragment of SREBP2 (SREBP2-N) or LacZ. **a–h** indicate western blot of **a**, **d** SREBP2, **b**, **c** PARP, **e** V5, **f** cleaved caspase-3, **g** caspase-7 (a 35-kDa proform and a 20-kDa cleaved form), and **h** HSP60. The lanes *1–12* represent (*1*, *5*) untreated HMO6 cells, and HMO6 cells treated for 1 h with (*2*) 10 μM FTY720-non-P, (*3*) 20 μM FTY720-non-P, (*4*) 3 μM simvastatin, and HMO6 cells pretreated for simvastatin starting at 12 h before a 6 h-exposure to FTY720-non-P, whose conditions are composed of (*6*) 3 μM simvastatin pretreatment alone, (*7*) 5 μM simvastatin pretreatment alone, (*8*) no simvastatin pretreatment and 5 μM FTY720-non-P exposure, (*9*) 3 μM simvastatin pretreatment and 5 μM FTY720-non-P exposure, and (*10*) 5 μM simvastatin pretreatment and 5 μM FTY720-non-P exposure, and HMO6 cells with overexpression of (*11*) V5-tagged LacZ or (*12*) SREBP2-N

SREBP activation is not a secondary phenomenon following caspase-3 activation. Furthermore, we found that activation of SREBP2 by overexpression of the N-terminal fragment of SREBP2 in HMO6 cells enhances the cleavage of PARP and caspase-3 in the absence of FTY720. Moreover, we found that pretreatment with simvastatin enhanced FTY720-non-P-induced apoptosis of HMO6 cells. Statins activate SREBP2 and induce apoptosis of various cells (Xia et al. 2001; Gibot et al. 2009). All of these observations suggest that the SREBP2-dependent signaling pathway is intrinsically proapoptotic, when it is aberrantly regulated.

A recent study showed that FTY720 inhibits intracellular transport of cholesterol to ER in human macrophages, being independent of S1P1 binding, indicating that FTY720-non-P certainly affects the cellular cholesterol processing (Blom et al. 2010). Importantly, cholesterol interacts specifically with sphingosine in human intestinal epithelial cells under physiological conditions (Garmy et al. 2005). S1P is intracellularly generated by sphingosine kinases SPHK1 and SPHK2 from sphingosine, a breakdown product of the cell membrane constituent sphingomyelin (Chi 2011). S1P and its synthetic analog FTY720-P share S1P1, S1P3, S1P4, and S1P5 expressed on the plasma membrane. All of these observations propose a possible scenario that excessive amounts of intracellular FTY720-non-P disturb the complex metabolic network of cholesterols and sphingolipids, resulting in activation of the SREBP2-dependent proapoptotic signaling pathway.

Acknowledgments This work was supported by grants from the Research on Intractable Diseases, the Ministry of Health, Labour and Welfare, Japan (H22-Nanchi-Ippan-136; H21-Nanchi-Ippan-201; H21-Nanchi Ippan-217; H21-Kokoro-Ippan-018) and the High-Tech Research Center Project (S0801043) and the Grant-in-Aid (C22500322), the Ministry of Education, Culture, Sports, Science and Technology (MEXT), Japan. The microarray data are available from Gene Expression Omnibus (GEO) under the accession number GSE28642.

References

Bandhuvula P, Tam YY, Oskouian B, Saba JD (2005) The immune modulator FTY720 inhibits sphingosine-1-phosphate lyase activity. J Biol Chem 280:33697–33700

Berdyshev EV, Gorshkova I, Skobeleva A, Bittman R, Lu X, Dudek SM, Mirzapoiazova T, Garcia JG, Natarajan V (2009) FTY720 inhibits ceramide synthases and up-regulates dihydrosphingosine 1-phosphate formation in human lung endothelial cells. J Biol Chem 284:5467–5477

Blom T, Bäck N, Mutka AL, Bittman R, Li Z, de Lera A, Kovanen PT, Diczfalusy U, Ikonen E (2010) FTY720 stimulates 27-hydroxycholesterol production and confers atheroprotective effects in human primary macrophages. Circ Res 106:720–729

Brinkmann V, Wilt C, Kristofic C, Nikolova Z, Hof RP, Chen S, Albert R, Cottens S (2001) FTY720: dissection of membrane receptor-operated, stereospecific effects on cell migration from receptor-independent antiproliferative and apoptotic effects. Transplant Proc 33:3078–3080

Brinkmann V, Billich A, Baumruker T, Heining P, Schmouder R, Francis G, Aradhye S, Burtin P (2010) Fingolimod (FTY720): discovery and development of an oral drug to treat multiple sclerosis. Nat Rev Drug Discov 9:883–897

Chi H (2011) Sphingosine-1-phosphate and immune regulation: trafficking and beyond. Trends Pharmacol Sci 32:16–24

Choi JW, Gardell SE, Herr DR, Rivera R, Lee CW, Noguchi K, Teo ST, Yung YC, Lu M, Kennedy G, Chun J (2011) FTY720 (fingolimod) efficacy in an animal model of multiple sclerosis requires astrocyte sphingosine 1-phosphate receptor 1 (S1P1) modulation. Proc Natl Acad Sci USA 108:751–756

Coelho RP, Payne SG, Bittman R, Spiegel S, Sato-Bigbee C (2007) The immunomodulator FTY720 has a direct cytoprotective effect in oligodendrocyte progenitors. J Pharmacol Exp Ther 323:626–635

da Huang W, Sherman BT, Lempicki RA (2009) Systematic and integrative analysis of large gene lists using DAVID bioinformatics resources. Nat Protoc 4:44–57

Dev KK, Mullershausen F, Mattes H, Kuhn RR, Bilbe G, Hoyer D, Mir A (2008) Brain sphingosine-1-phosphate receptors: implication for FTY720 in the treatment of multiple sclerosis. Pharmacol Ther 117:77–93

Durafourt BA, Lambert C, Johnson TA, Blain M, Bar-Or A, Antel JP (2011) Differential responses of human microglia and blood-derived myeloid cells to FTY720. J Neuroimmunol 230:10–16

Garmy N, Taïeb N, Yahi N, Fantini J (2005) Interaction of cholesterol with sphingosine: physicochemical characterization and impact on intestinal absorption. J Lipid Res 46:36–45

Gibot L, Follet J, Metges JP, Auvray P, Simon B, Corcos L, Le Jossic-Corcos C (2009) Human caspase 7 is positively controlled by SREBP-1 and SREBP-2. Biochem J 420:473–483

Higgins ME, Ioannou YA (2001) Apoptosis-induced release of mature sterol regulatory element-binding proteins activates sterol-responsive genes. J Lipid Res 42:1939–1946

Hisano Y, Kobayashi N, Kawahara A, Yamaguchi A, Nishi T (2011) The sphingosine 1-phosphate transporter, SPNS2, functions as a transporter of the phosphorylated form of the immunomodulating agent FTY720. J Biol Chem 286:1758–1766

Jack C, Ruffini F, Bar-Or A, Antel JP (2005) Microglia and multiple sclerosis. J Neurosci Res 81:363–373

Jin Y, Zollinger M, Borell H, Zimmerlin A, Patten CJ (2011) CYP4F enzymes are responsible for the elimination of fingolimod (FTY720), a novel treatment of relapsing multiple sclerosis. Drug Metab Dispos 39:191–198

Kappos L, Antel J, Comi G, Montalban X, O'Connor P, Polman CH, Haas T, Korn AA, Karlsson G, Radue EW, FTY720 D2201 Study Group (2006) Oral fingolimod (FTY720) for relapsing multiple sclerosis. N Engl J Med 355:1124–1140

Lee TK, Man K, Ho JW, Sun CK, Ng KT, Wang XH, Wong YC, Ng IO, Xu R, Fan ST (2004) FTY720 induces apoptosis of human hepatoma cell lines through PI3-K-mediated Akt dephosphorylation. Carcinogenesis 25:2397–2405

Liu Q, Alinari L, Chen CS, Yan F, Dalton JT, Lapalombella R, Zhang X, Mani R, Lin T, Byrd JC, Baiocchi RA, Muthusamy N (2010) FTY720 shows promising in vitro and in vivo preclinical activity by downmodulating cyclin D1 and phospho-Akt in mantle cell lymphoma. Clin Cancer Res 16:3182–3192

Matsuda S, Minowa A, Suzuki S, Koyasu S (1999) Differential activation of c-Jun NH2-terminal kinase and p38 pathways during FTY720-induced apoptosis of T lymphocytes that is suppressed by the extracellular signal-regulated kinase pathway. J Immunol 162:3321–3326

Matsuoka Y, Nagahara Y, Ikekita M, Shinomiya T (2003) A novel immunosuppressive agent FTY720 induced Akt dephosphorylation in leukemia cells. Br J Pharmacol 138:1303–1312

Miron VE, Jung CG, Kim HJ, Kennedy TE, Soliven B, Antel JP (2008) FTY720 modulates human oligodendrocyte progenitor process extension and survival. Ann Neurol 63:61–71

Miron VE, Ludwin SK, Darlington PJ, Jarjour AA, Soliven B, Kennedy TE, Antel JP (2010) Fingolimod (FTY720) enhances remyelination following demyelination of organotypic cerebellar slices. Am J Pathol 176:2682–2694

Mullershausen F, Zecri F, Cetin C, Billich A, Guerini D, Seuwen K (2009) Persistent signaling induced by FTY720-phosphate is mediated by internalized S1P1 receptors. Nat Chem Biol 5: 428–434

Nagai A, Nakagawa E, Hatori K, Choi HB, McLarnon JG, Lee MA, Kim SU (2001) Generation and characterization of immortalized human microglial cell lines: expression of cytokines and chemokines. Neurobiol Dis 8:1057–1068

Nagaoka Y, Otsuki K, Fujita T, Uesato S (2008) Effects of phosphorylation of immunomodulatory agent FTY720 (fingolimod) on antiproliferative activity against breast and colon cancer cells. Biol Pharm Bull 31:1177–1181

Narantuya D, Nagai A, Sheikh AM, Masuda J, Kobayashi S, Yamaguchi S, Kim SU (2010) Human microglia transplanted in rat focal ischemia brain induce neuroprotection and behavioral improvement. PLoS One 5:e11746

Payne SG, Oskeritzian CA, Griffiths R, Subramanian P, Barbour SE, Chalfant CE, Milstien S, Spiegel S (2007) The immunosuppressant drug FTY720 inhibits cytosolic phospholipase A2 independently of sphingosine-1-phosphate receptors. Blood 109: 1077–1085

Potteck H, Nieuwenhuis B, Lüth A, van der Giet M, Kleuser B (2010) Phosphorylation of the immunomodulator FTY720 inhibits programmed cell death of fibroblasts via the S1P3 receptor subtype and Bcl-2 activation. Cell Physiol Biochem 26:67–78

Sato R (2010) Sterol metabolism and SREBP activation. Arch Biochem Biophys 501:177–181

Satoh J, Tabunoki H, Arima K (2009) Molecular network analysis suggests aberrant CREB-mediated gene regulation in the Alzheimer disease hippocampus. Dis Markers 27:239–252

Sensken SC, Gräler MH (2010) Down-regulation of S1P1 receptor surface expression by protein kinase C inhibition. J Biol Chem 285:6298–6307

Sonoda Y, Yamamoto D, Sakurai S, Hasegawa M, Aizu-Yokota E, Momoi T, Kasahara T (2001) FTY720, a novel immunosuppressive agent, induces apoptosis in human glioma cells. Biochem Biophys Res Commun 281:282–288

Van Doorn R, Van Horssen J, Verzijl D, Witte M, Ronken E, Van Het Hof B, Lakeman K, Dijkstra CD, Van Der Valk P, Reijerkerk A, Alewijnse AE, Peters SL, De Vries HE (2010) Sphingosine 1-phosphate receptor 1 and 3 are upregulated in multiple sclerosis lesions. Glia 58:1465–1476

Wang JD, Takahara S, Nonomura N, Ichimaru N, Toki K, Azuma H, Matsumiya K, Okuyama A, Suzuki S (1999) Early induction of apoptosis in androgen-independent prostate cancer cell line by FTY720 requires caspase-3 activation. Prostate 40:50–55

Wei Y, Yemisci M, Kim HH, Yung LM, Shin HK, Hwang SK, Guo S, Qin T, Alsharif N, Brinkmann V, Liao JK, Lo EH, Waeber C (2011) Fingolimod provides long-term protection in rodent models of cerebral ischemia. Ann Neurol 69:119–129

Woodcock JM, Ma Y, Coolen C, Pham D, Jones C, Lopez AF, Pitson SM (2010) Sphingosine and FTY720 directly bind pro-survival 14-3-3 proteins to regulate their function. Cell Signal 22: 1291–1299

Xia Z, Tan MM, Wong WW, Dimitroulakos J, Minden MD, Penn LZ (2001) Blocking protein geranylgeranylation is essential for lovastatin-induced apoptosis of human acute myeloid leukemia cells. Leukemia 15:1398–1407

Zhang Z, Zhang Z, Fauser U, Artelt M, Burnet M, Schluesener HJ (2007) FTY720 attenuates accumulation of EMAP-II+ and MHC-II+ monocytes in early lesions of rat traumatic brain injury. J Cell Mol Med 11:307–314

European Journal of Neurology 2010, **18:** 1179–1183 doi:10.1111/j.1468-1331.2010.03311.x

SHORT COMMUNICATION

Nasu–Hakola disease with a splicing mutation of TREM2 in a Japanese family

Y. Numasawa[a], C. Yamaura[a], S. Ishihara[a], S. Shintani[a], M. Yamazaki[b], H. Tabunoki[c] and J.-I. Satoh[c]

[a]*Department of Neurology, Toride Kyodo General Hospital, Toride City, Ibaraki;* [b]*The 2nd Department of Internal Medicine, Nippon Medical School, Bunkyo-ku, Tokyo; and* [c]*Department of Bioinformatics and Molecular Neuropathology, Meiji Pharmaceutical University, Kiyose, Tokyo, Japan*

Keywords:
exon 3 skipping, Nasu–Hakola disease, PLOSL, transcriptome, TREM2 mutation

Received 28 September 2010
Accepted 18 November 2010

Background: Nasu–Hakola disease (NHD) is a rare autosomal recessive disorder, characterized by a combination of progressive presenile dementia and formation of multifocal bone cysts, caused by genetic mutations of DAP12 and TREM2, which constitute a receptor/adapter signaling complex expressed on osteoclasts, dendritic cells, macrophages, and microglia. No Japanese patients with TREM2 mutations have been reported previously.

Methods: We reported three siblings affected with NHD in a Japanese family. Amongst them, two died of NHD during the fourth decade of life. The analysis of genomic DNA, cDNA cloning, and western blot of lymphocyte proteins was performed on samples of the living patient. The transcriptome was studied in the autopsied brain of one patient.

Results: We identified a homozygous conversion of a single nucleotide T to C at the second position of intron 3 in the splice-donor consensus site (c.482 + 2T > C) of the TREM2 gene, resulting in exon 3 skipping and aberrant expression of truncated proteins. We identified 136 upregulated genes involved in inflammatory response and immune cell trafficking and 188 downregulated genes including a battery of GABA receptor subunits and synaptic proteins in the patient's brain.

Conclusions: This is the first report of a Japanese NHD family caused by a splicing mutation of TREM2 that induces both neuroinflammation and neurodegeneration.

Introduction

Nasu–Hakola disease (NHD; OMIM 221770), also designated polycystic lipomembranous osteodysplasia with sclerosing leukoencephalopathy (PLOSL), is a rare autosomal recessive disorder, characterized by a combination of progressive presenile dementia and formation of multifocal bone cysts [1]. The clinical course of NHD is divided into four stages: (i) the latent stage with normal early development, (ii) the osseous stage beginning at the third decade of life, characterized by pathological bone fractures, (iii) the early neuropsychiatric stage occurring at the fourth decade of life, presenting with a frontal lobe syndrome, and (iv) the late neuropsychiatric stage, characterized by profound dementia, and death usually by age 50 years [1].

Nasu–Hakola disease is caused by a structural defect in one of the two genes, DAP12 (TYROBP) or TREM2, both of which induce a clinicopathologically identical phenotype [2,3]. DAP12, expressed as a disulfide-bonded homodimer on NK cells, monocytes/macrophages, dendritic cells, osteoclasts, and brain microglia, constitutes a transmembrane adaptor that non-covalently associates with several cell-surface receptors, including TREM2, TREM1, NCR2 (NKp44), SIRPB1, and MDL1, and transmits activating or inhibitory signals depending on the avidity of their ligands. The TREM2/DAP12 complex regulates key signaling events involved in immune responses, differentiation of dendritic cells and osteoclasts, and phagocytic activity of microglia. Until present, 17 different NHD-causing mutations have been identified in

Correspondence: J.-I. Satoh, MD, PhD, Department of Bioinformatics and Molecular Neuropathology, Meiji Pharmaceutical University, 2-522-1 Noshio, Kiyose, Tokyo 204-8588, Japan (tel.: +81 42 495 8678; fax: +81 42 495 8678; e-mail: satoj@my-pharm.ac.jp).

either DAP12 or TREM2 [2,3]. DAP12 mutations are predominant in Finnish and Japanese, whilst TREM2 mutations are distributed widely. However, no NHD patients with TREM2 mutations have been previously found in Japan. In this study, we describe the first case of a Japanese NHD family caused by a splicing mutation of TREM2.

Methods

Mutation analysis

After written informed consent was obtained, high molecular weight genomic DNA was extracted from whole peripheral blood. The Ethics Committee of MPU approved this study. All five exons and 5′ and 3′ flanking regions of the TREM2 gene were amplified by PCR using primer sets following: exon 1, 5′caccgccttcataattcaccc3′ and 5′gactcctcctcccctctgtc3′; exon 2, 5′agtgggtggttctgcacac3′ and 5′gctccttcagggcaggattt3′; exon 3, 5′gctctagttgccttgtaatttgtagt3′ and 5′agtgtaatgacctgatccacatagga3′; and exons 4 and 5, 5′tcttccttcacgtgtctctcagcc3′ and 5′aaggcccatcccagggatggtgct3′. The purified PCR products were processed for direct sequencing on the 3730xl DNA Analyzer (Applied Biosystems, Foster City, CA, USA). cDNA and protein extract were prepared from peripheral blood mononuclear cells (PBMC). The junctional sequence of exons 3 and 4 or the sequence spanning the entire open-reading frame (ORF) and 5′ and 3′ flanking regions amplified by PCR of cDNA was cloned in the pcDNA4/HisMax-TOPO vector (Invitrogen, Carlsbad, CA, USA) and processed for sequencing analysis.

DNA microarray and molecular network analysis

Total RNA was isolated from a small piece derived from the fragmented bulk of autopsied frozen frontal lobe tissues of the patient 1. In parallel, we studied gene expression profile of the normal human frontal lobe RNA (636563; Clontech, Mountain View, CA, USA), pooled from unspecified regions isolated from four male/female Caucasians of ages 32–61 died of sudden death, serving as a control. The RNA integrity number (RIN) of total RNA on 2100 Bioanalyzer (Agilent Technologies, Palo Alto, CA, USA) was 6.1 for the control and 6.7 for the patient's sample, respectively. One hundred ng of total RNA was processed for microarray analysis with Human Gene 1.0 ST Array (Affymetrix, Santa Clara, CA, USA) containing 28 869 genes. The CEL file data were normalized by the robust multiarray average (RMA) method. When compared with gene expression levels in the control, the genes showing upregulation greater than fourfold or downregulation smaller than 0.1-fold were defined as differentially expressed genes. To identify biologically relevant molecular pathways, we utilized Ingenuity Pathways Analysis (IPA) tool (Ingenuity Systems). By uploading the list of Gene IDs and expression values, the network-generation algorithm identified focused genes integrated in a global molecular network with the score *P*-value reflecting the statistical significance of association between the genes and the networks by the Fisher's exact test.

Results

The Japanese NHD family

A 36-year-old woman (the patient 3; the index) was admitted to the hospital because of epileptic seizure. Her parents are consanguineous. The patient has three siblings. The eldest brother (the patient 1) developed intractable epileptic seizures at age 33 was diagnosed as having NHD, became bedridden, and died at age 39 because of decubital infection in a different hospital, where the autopsy was performed. The second elder brother (the patient 2) was also clinically diagnosed as NHD in another hospital, and lead to sudden death of an unknown cause at age 31. The elder sister at age 44 is currently healthy.

The patient 3 has been normal until age 34, when she gradually began to show personality change, characterized by laziness, lack of concentration and insight, and loss of judgment and social inhibitions. At age 36, she showed a sign of apathy and memory disturbance and was affected with generalized tonic-clonic seizures. On admission, she was postictal but neurologically normal except for diffuse hyperactive deep-tendon reflexes and occasional myoclonic jerks. She showed a profound decrease in the score (seven of 30) on examination of a revised version of Hasegawa's Dementia Scale.

X-ray examinations showed multifocal radiolucent lesions distributed in distal ends of humerus, radius, femur, tibia, and metatarsal bone (Fig. 1a). Brain CT revealed bilateral calcification of the basal ganglia (Fig. 1b). Brain MRI showed moderate atrophy of the frontotemporal cortex and marked dilatation of the lateral ventricle on a T2-weighted image (Fig. 1c). 99mTc-ECD SPECT showed moderate hypoperfusion in the frontotemporal cortex with preservation of the cerebral blood flow in the basal ganglia (Fig. 1d). An EEG displayed sporadic spike waves in diffuse slow activities. The routine laboratory examination of blood and cerebrospinal fluid was normal. All of neurological and radiological findings described earlier supported a clinical diagnosis of NHD.

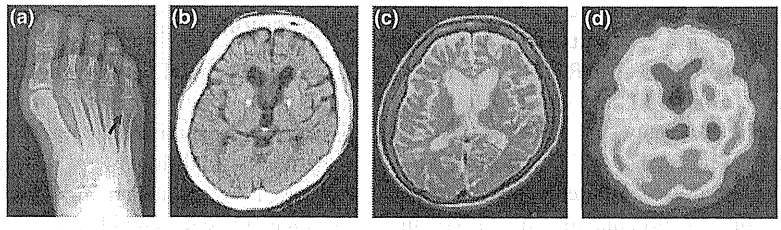

Figure 1 Neuroradiological features of the patient 3. (a) X-ray film. A cystic lesion in the fifth metatarsal bone (arrow). (b) Brain CT. High density lesions in the bilateral basal ganglia. (c) Brain MRI. Moderate atrophy of the frontotemporal cortex and marked dilatation of the lateral ventricle on an axial T2-weighted image (TR: 4500 ms, TE: 98 ms). (d) 99mTc-ECD SPECT. Moderate hypoperfusion in the frontotemporal cortex with preservation of the cerebral blood flow in the basal ganglia.

Identification of a splicing mutation in intron 3 of the TREM2 gene

In the patient 3, we identified a homozygous conversion of a single nucleotide T to C at the second position of intron 3 in the splice-donor consensus site (c.482+2T>C) of the TREM2 gene (Fig. 2a). No mutations were found in the DAP12 gene. The junctional sequence between exon 3 and exon 4 was not detected by PCR of cDNA of the patient 3 (Fig. 2b, lane 1). By western blot, a 38-kDa full-length TREM2 protein was identified in PBMC of a normal subject (Fig. 2c, lane 2), whereas 27-kDa and 24-kDa truncated TREM2 proteins were detected in the patient 3 (Fig. 2c, lane 1).

The cloning and sequencing of the TREM2 ORF verified exon 3 skipping in combination with deletion of exon 2 and/or exon 4, followed by emergence of the premature or original stop codons (Fig. S1, panels a–d). The exon 3-skipped genes are predicted to encode four distinct truncated proteins, composed of 157 amino acids (35-kDa), 135 amino acids (28-kDa), amino acids 40 (11-kDa), or 18 amino acids (0.5-kDa), tentatively named as variant 1, 2, 3, or 4, respectively. The wild-type full-length TREM2 protein consists of 230 amino acids, composed of a 13-amino acid signal peptide, followed by an 154-amino acid extracellular immunoglobulin superfamily (Ig-SF) domain pivotal for binding to the ligand, a 33-amino acid transmembrane (TM) domain essential for binding to DAP12, and a 30-amino acid cytoplasmic domain. InterProScan (http://www.ebi.ac.uk/Tools/InterProScan) search indicated that variants 1 and 2 have the Ig-SF domain but do not have the TM domain, whilst variants 3 and 4 lack both Ig-SF and TM domains, suggesting that all of these variants are non-functional. It remains unknown whether these variants expressed as truncated proteins produce a dominant negative effect on TREM2/DAP12 signaling.

Gene expression analysis of autopsied brain tissues

We again identified the c.482+2T>C mutation in the genomic DNA isolated from the brain of the patient 1. The transcriptome analysis of the brain identified totally 136 upregulated genes (Table S1) and 188 downregulated genes (Table S2). Macrophage/microglia marker genes, such as CD163, MSR1, and CD68,

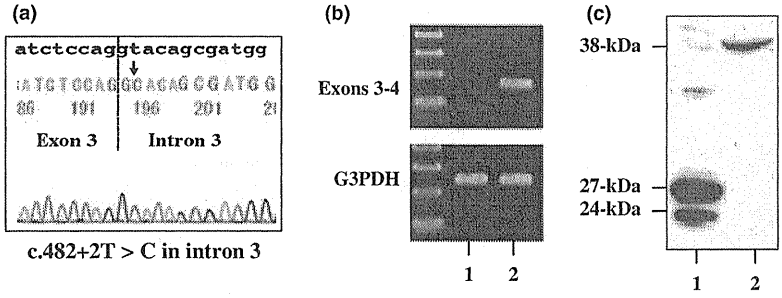

Figure 2 TREM2 mutation of the patient 3. (a) Direct sequencing. PCR and sequencing of all five exons and exon–intron boundaries of the TREM2 gene identified a homozygous conversion of a single nucleotide T to C in the splice-donor consensus site at the second position of intron 3 (c.482+2T>C). (b) The junctional sequence of exons 3 and 4. The junctional sequence of exons 3 and 4 of TREM2 (upper panel) and G3PDH (lower panel) amplified by PCR from cDNA of PBMC. The lanes (1, 2) represent (1) the patient and (2) normal subject. (c) TREM2 protein expression. Western blot of PBMC protein with anti-TREM2 antibody (HPA010917, Sigma). The lanes (1, 2) represent (1) the patient and (2) normal subject.

were greatly upregulated, whereas the genes encoding nine different GABA receptor subunits, such as GABRG2, GABRA1, GABRB2, GABRA2, GABRA4, GABRA3, GABRA5, GABRB3, and GABRB1, along with various synaptic components, such as SYT1, SNAP25, SV2B, SYNPR, SYT4, SYT13, SYN2, and SYT5, were coordinately downregulated. Top 10 genes, either upregulated or downregulated, are listed in Table 1. Upregulation of RGS1 and CD163 and downregulation of GABRG2 and SYT1 were validated by qRT-PCR analysis (Fig. S2). With respect to neuronal and glial marker genes, the fold change of gene expression levels in the patient's brain vs. the control is NEFH (neurons), 0.30; PVALB (GABA neurons), 0.18; GFAP (astrocytes), 2.57; MBP (oligodendrocytes), 1.60; and G3PDH (housekeeping gene), 0.63, suggesting marked loss of neurons with enhanced astrogliosis in the NHD brain at a terminal stage.

By IPA, the set of 136 upregulated genes constituted a highly complex network of 64 focused genes showing the most significant relationship with inflammatory response, cellular movement, and immune cell trafficking (P = 1.00E-116) (Fig. S3a), whilst 188 downregulated genes formed the network of 91 focused genes showing the most significant relationship with cell-to-cell signaling and interaction, nervous system development and function, and genetic disorder (P = 1.00E-168) (Fig. S3b).

Discussion

Here, we described the first report of a Japanese NHD family caused by a splicing mutation of TREM2. Three patients showed clinical features typical of NHD, and the patient 1 and the patient 3 exhibited a homozygous c.482+2T>C mutation inducing exon 3 skipping of the TREM2 gene. The identical mutation was reported previously in two patients of an Italian family [2–4]. Until present, 20 patients with 11 different TREM2 mutations have been reported worldwide, including one patient with G40T (Q14stop), four with C97T (Q33stop), one with G132A (W44stop), two with G233A (W78stop), one with 267delG (frameshift followed by premature termination), one with 313delG (frameshift followed by premature termination), two with T377G (V126G), one with A401G (D134G), two with G558T (K86N), two with c.482+2T>C (splicing mutation), or three with c.40+3delAGG at the third position of intron 1 in the splice-donor consensus site (splicing mutation) [2–6].

TREM2 is expressed exclusively in osteoclasts, dendritic cells, tissue-infiltrating macrophages, and a subpopulation of microglia, located in the Golgi complex and exocytic vesicles, on cell-surface membranes, and in part released extracellularly [7]. TREM2 expressed on mouse microglia plays a key role in tissue debris clearance and resolution of inflammation [8]. We

Table 1 Top 10 upregulated and downregulated genes in the brain of a Nasu–Hakola disease patient with TREM2 mutation

Rank	Fold change	Gene ID	Gene symbol	Gene description
Upregulated genes				
1	40.2	5996	RGS1	Regulator of G-protein signaling 1
2	13.3	9103	FCGR2C	Fc fragment of IgG, low affinity IIc, receptor for (CD32)
3	13.2	9332	CD163	CD163 molecule
4	12.9	312	ANXA13	Annexin A13
5	12.1	4640	MYO1A	Myosin IA
6	11.6	7852	CXCR4	Chemokine (C-X-C motif) receptor 4
7	11.5	118932	ANKRD22	Ankyrin repeat domain 22
8	10.7	84689	MS4A14	Membrane-spanning 4-domains, subfamily A, member 14
9	10.7	1610	DAO	D-amino acid oxidase
10	10.4	3606	IL18	Interleukin 18 (interferon-gamma-inducing factor)
Downregulated genes				
1	0.008	7447	VSNL1	Visinin-like 1
2	0.010	2566	GABRG2	Gamma-aminobutyric acid (GABA) A receptor, gamma 2
3	0.010	2554	GABRA1	Gamma-aminobutyric acid (GABA) A receptor, alpha 1
4	0.011	5999	RGS4	Regulator of G-protein signaling 4
5	0.011	6857	SYT1	Synaptotagmin I
6	0.012	6616	SNAP25	Synaptosomal-associated protein, 25kDa
7	0.014	8507	ENC1	Ectodermal-neural cortex (with BTB-like domain)
8	0.016	114569	MAL2	Mal, T-cell differentiation protein 2
9	0.018	4753	NELL2	NEL-like 2 (chicken)
10	0.018	9899	SV2B	Synaptic vesicle glycoprotein 2B

The transcriptome of frontal lobe tissues of the patient 1 was studied using Human Gene 1.0 ST array (Affymetrix). When compared with the gene expression levels in the control, top 10 upregulated and downregulated genes are listed with fold change, Entrez Gene ID, gene symbol, and description. See Tables S1 and S2 for the entire list.

for the first time characterized the genome-wide transcriptome of the NHD brain, although the case, the control, and the region of the brain, possibly affecting gene expression profiles, are fairly limited because of restricted availability of the samples. We identified a panel of upregulated genes closely associated with inflammatory response and immune cell function, and downregulated genes related to the nervous system function, indicating a concurrence of neuroinflammatory and neurodegenerative events in NHD brains.

Acknowledgements

This work was supported by grants to J-IS from Research on Intractable Diseases, the Ministry of Health, Labour and Welfare, Japan (H22-Nanchi-Ippan-136), and the High-Tech Research Center Project (S0801043) and the Grant-in-Aid (C22500322), the Ministry of Education, Culture, Sports, Science and Technology (MEXT), Japan. The gene sequence data are registered in GenBank with the accession number AB601768, and the microarray data are available from Gene Expression Omnibus (GEO) under the accession number GSE25496.

Disclosure of conflict of interest

The authors declare no financial or other conflict of interests.

References

1. Bianchin MM, Capella HM, Chaves DL, *et al.* Nasu–Hakola disease (polycystic lipomembranous osteodysplasia with sclerosing leukoencephalopathy-PLOSL): a dementia associated with bone cystic lesions. From clinical to genetic and molecular aspects. *Cell Mol Neurobiol* 2004; **24:** 1–24.
2. Klünemann HH, Ridha BH, Magy L, *et al.* The genetic causes of basal ganglia calcification, dementia, and bone cysts: DAP12 and TREM2. *Neurology* 2005; **64:** 1502–1507.
3. Paloneva J, Manninen T, Christman G, *et al.* Mutations in two genes encoding different subunits of a receptor signaling complex result in an identical disease phenotype. *Am J Hum Genet* 2002; **71:** 656–662.
4. Salmaggi A, Maccagnano E, Musso A, Di Lena L, Paloneva J, Boiardi A. An Italian family with Nasu–Hakola disease. *J Neurol* 2003; **250:** 878–880.
5. Soragna D, Papi L, Ratti MT, Sestini R, Tupler R, Montalbetti L. An Italian family affected by Nasu–Hakola disease with a novel genetic mutation in the TREM2 gene. *J Neurol Neurosurg Psychiatry* 2003; **74:** 825–826.
6. Chouery E, Delague V, Bergougnoux A, Koussa S, Serre JL, Mégarbané A. Mutations in TREM2 lead to pure early-onset dementia without bone cysts. *Hum Mutat* 2008; **29:** E194–E204.
7. Sessa G, Podini P, Mariani M, *et al.* Distribution and signaling of TREM2/DAP12, the receptor system mutated in human polycystic lipomembraneous osteodysplasia with sclerosing leukoencephalopathy dementia. *Eur J Neurosci* 2004; **20:** 2617–2628.
8. Takahashi K, Rochford CD, Neumann H. Clearance of apoptotic neurons without inflammation by microglial triggering receptor expressed on myeloid cells-2. *J Exp Med* 2005; **201:** 647–657.

Supporting Information

Additional Supporting Information may be found in the online version of this article:

Figure S1. The c.482 + 2T > C mutation induces exon 3 skipping. The ORF of TREM2 amplified by PCR was cloned in the vector. Four distinct clones were processed for sequencing analysis. The panels (a–d) represent (a) variant 1 with deletion of exon 3, composed of 157 amino acids, (b) variant 2 with deletion of exons 3 and 4, composed of 135 amino acids, (c) variant 3 with deletion of exons 2 and 3, composed of 40 amino acids, and (d) variant 4 with deletion of exons 2, 3, and 4, composed of 18 amino acids. The stop codon is underlined in variants 2 and 4.

Figure S2. Validation of microarray data by qRT-PCR. The microarray data was validated by quantitative RT-PCR on LightCycler ST300 (Roche Diagnostics). The panels represent (a) RGS1, (b) CD163, (c) GABRG2, and (d) SYT1. The expression levels of each gene were standardized against those of G3PDH. Frontal lobe cDNA of NC (the normal control), NHD (the patient 1), ALS1 and ALS2 (two patients with amyotrophic lateral sclerosis), and AD1 and AD2 (two patients with Alzheimer disease) were analyzed.

Figure S3. Molecular network of 136 upregulated and 188 downregulated genes in the brain of a NHD patient with TREM2 mutation. By Ingenuity Pathways Analysis of brain transcriptome data of the patient 1, 136 upregulated genes constitute the network of 64 focused genes (red) that has the most significant relationship with inflammatory response, cellular movement, and immune cell trafficking (P = 1.00E-116) (panel a), whilst 188 downregulated genes constitute the network of 91 focused genes (green) that has the most significant relationship with cell-to-cell signaling and interaction, nervous system development and function, and genetic disorder (P = 1.00E-168) (panel b).

Table S1. The list of 136 upregulated genes in the brain of a NHD patient with TREM2 mutation.

Table S2. The list of 188 downregulated genes in the brain of a NHD patient with TREM2 mutation.

Please note: Wiley-Blackwell is not responsible for the content or functionality of any supporting materials supplied by the authors. Any queries (other than missing material) should be directed to the corresponding author for the article.

INTERNAL MEDICINE

□ CASE REPORT □

A Japanese Case with Nasu-Hakola Disease of DAP12 Gene Mutation Exhibiting Precuneus Hypoperfusion

Kiyotaka Nakamagoe[1], Ayako Shioya[1], Tetsuto Yamaguchi[1], Hiroyuki Takahashi[1], Reiko Koide[1], Tatsuya Monzen[2], Jun-ichi Satoh[3] and Akira Tamaoka[1]

Abstract

A 38-year-old Japanese man with Nasu-Hakola disease (NHD) had repeated pathological fractures and frontal lobe symptoms which developed when he was 18 and 26 years old, respectively. Neuropsychological testing showed memory impairment, and in particular, visuo-spatial memory at the age of 35. Furthermore, single-photon emission computed tomography revealed precuneus hypoperfusion. The patient later suffered prolonged convulsive seizures, which left him in a persistent vegetative state. Genetic testing confirmed a heterozygous mutation in the DAP12 gene (a single-base deletion of 141 G in exon 3) specific to NHD. Precuneus dysfunction might contribute to characteristic memory impairment of NHD.

Key words: Nasu-Hakola disease, DAP12, TREM2, SPECT, MRI, precuneus

(Intern Med 50: 2839-2844, 2011)
(DOI: 10.2169/internalmedicine.50.5891)

Introduction

Nase-Hakola disease (NHD), an extremely rare autosomal recessive inherited disease also referred to as polycystic lipomembranous osteodysplasia with sclerosing leukoencephalopathy (PLOSL), occurs most commonly among the Japanese and Finnish populations. Our PubMed literature search identified approximately 50 reported cases of NHD.

The cardinal symptoms include multiple bone cysts accompanied by pathological fractures and early-onset dementia induced by leukoencephalopathy. The clinical course of NHD follows four stages: latent, osseous, early neurological, and late neurological stages (1-5). The latent stage generally takes place before the patient reaches the age of 20. The osseous stage, which begins after the patient is 20, is characterized by the development of multiple bone cysts, which occur most frequently at the epiphyses of long tubular bones, accompanied by bone pain and repeated pathological fractures. The early neurological stage starts after the patient is 30, with the manifestation of frontal lobe symptoms, including disinhibition, euphoria, and personality disorder, as well as the onset of epileptic seizures. The late neurological stage sets in after the patient is 40, and the patient develops a rapidly progressive, profound dementia, and eventually becomes bedridden. Most patients die in their 30s or 40s.

According to previous reports, the homozygous deletion or point mutation of DAP12 (TYRO protein tyrosine kinase-binding protein, TYROBP) or the triggering receptor expressed on myeloid cells 2 (TREM2) is the typical genetic defect observed in NHD (3, 4, 6, 7). Furthermore, Kuroda et al reported a case in which a compound heterozygote of a defective DAP12 gene was detected (8). Genetic mutations of DAP12 and TREM2 lead to losses of function expressed in microglia in the brain and osteoclasts in the bone, which cause symptoms to appear in the central nervous system and bone.

NHD can be diagnosed with relative ease when it is accompanied by bone lesions, in which case the presence of polycystic lipomembranous osteodysplasia, which is specific to NHD, in the bone biopsy specimen confirms the diagnosis. However, without such bone lesions, diagnosis can be very difficult. According to Chouery et al, some patients in whom the mutation of the TREM2 gene was present developed early-onset dementia without exhibiting bone lesions (9). In such patients, genetic testing may be needed to

[1]Department of Neurology, Institute of Clinical Medicine, University of Tsukuba, Japan, [2]Department of Neurology, Ushiku Aiwa General Hospital, Japan and [3]Department of Bioinformatics and Molecular Neuropathology, Meiji Pharmaceutical University, Japan
Received for publication May 25, 2011; Accepted for publication August 15, 2011
Correspondence to Dr. Kiyotaka Nakamagoe, Nakamagoek@md.tsukuba.ac.jp

Table 1. Summary of Neuropsychological Tests

Neuropsychological Tests	Results
Mini-Mental State Examination (MMSE)	28/30 (errors on calculation and memory)
Wechsler Memory Scale-Revised (WMS-R; Index scores less than 85 indicate abnormal decline.)	Verbal Memory Index: 82 Visual Memory Index: <50 General Memory Index: 65 Attention/Concentration: 73 Delayed Memory: <50
Alzheimer's Disease Assessment Scale-cognitive component-Japanese version (ADAS-J cog.)	9/70
Clock Drawing Test	Error in standard version. Improvement in copied version.
Verbal Fluency Test	Difficulty in recalling words with initial Japanese letter, *ka*.

The testing was performed when the patient was 35 years old, before the onset of convulsive seizures. The profile shows the impairment in memory dysfunction (especially, visuospatial memory) and frontal dysfunction, although overall cognitive function (by MMSE) was shown to be still intact

arrive at a diagnosis of NHD.

Recent research has revealed an immune abnormality induced by genetic mutations associated with NHD (5, 10). In this paper, we report a case of NHD exhibiting a defective DAP12 gene with a focus on the relationship between clinical symptoms and image findings.

Case Report

The present case is a 38-year-old man. In his family history, his brother, who had multiple bone cysts and was suspected of having NHD, died in a traffic accident at the age of 19. The present patient had previously been healthy. At the age of 18, he experienced pain in the joints of both legs and had repeated pathological fractures. His X-rays showed multiple cystic radiolucent areas at the epiphyses of both legs and thickening of the trabecular bone. A bone biopsy, performed following autologous transplantation of the bones of both ankles, revealed polycystic lipomembranous osteodysplasia. Signs of disinhibition, personality changes, and behavioral abnormalities became evident when the patient was 26. Particularly abnormal behaviors, such as stealing and the reckless borrowing of money, escalated over time. T2-enhanced brain MRI images taken when the patient was 34 years old revealed diffuse high-intensity areas in the white matter as well as hippocampal atrophy. Neuropsychological tests performed when the patient was 35 showed higher-order cognitive dysfunction, including memory impairment (Table 1). Nine months after the testing, the patient had generalized seizures and subsequently received the antiepileptic agent phenytoin. Later, hypobulia became evident, and the patient became withdrawn. However, he was still able to perform daily activities, such as eating and walking. At the age of 36, he was admitted to our hospital immediately after having generalized tonic-clonic seizures, which resulted in prolonged convulsive seizures.

Physical findings on admission: The patient exhibited profoundly impaired consciousness with a score of 4 (E1, V1, M3) on the Glasgow Coma Scale. The size of both pupils was 2 mm and the light reflexes were absent from both eyes. The deep tendon reflexes were exaggerated in all limbs. Foot and knee cloni were positive bilaterally. Both Babinski and Chaddock reflexes were positive bilaterally. The palmomental reflex was also positive. Furthermore, the patient had double incontinence.

Disease progression after admission: The patient was put on a mechanical ventilator. Intravenous phenytoin and continuous intravenous midazolam infusion were initiated to treat prolonged generalized tonic-clonic seizures. Shortly afterwards, the generalized seizures disappeared and never returned. The patient had only transient episodes of partial seizures of the left upper limb. As the patient's condition improved, he was weaned from the mechanical ventilator on the 11th day of hospitalization. Around that time, the patient showed decerebrate rigidity. The convulsions were controlled by administration of 500 mg/day phenytoin via a gastric tube. Since that time the patient remained in a persistent vegetative state for over one year with no sign of improvement in the level of consciousness.

Neuropsychological testing was administered when the patient was 35 years old, prior to the first episode of convulsive seizures (Table 1). The patient scored 28 on the Mini-Mental State Examination (MMSE), indicating normal overall cognitive function. He made some errors on the items related to calculation and memory. On the Wechsler Memory Scale-Revised (WMS-R), the patient disclosed memory impairment in all indexes (less than 85), among which the scores were extremely low in visual memory and delayed memory (less than 50). On the Clock Drawing Test (CDT), the patient could not image the clock face exactly and hesitated to draw by organizing the parts of the clock; however, he could copy the clock face when he was shown a clock drawn by the tester, indicating that his error in CDT was not due to constructive apraxia but frontal executive dysfunction and memory dysfunction. There was also evidence of frontal lobe dysfunction, i.e., difficulty in verbal fluency task (recalling words with Japanese *ka* as the initial letter). With these results, the neuropsychological profile of this case resembles those often observed in patients with mild cognitive impairment (MCI), i.e., normal overall cognitive function with an abnormal decline in memory and frontal function; however, there is an additional striking feature

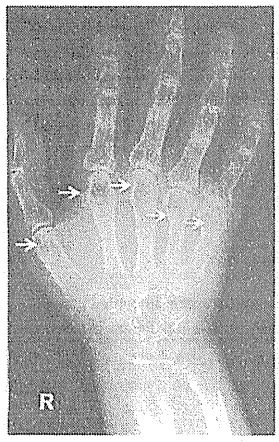

Figure 1. Plain X-ray images of hands and fingers. Multiple bone cysts were found at the epiphyses (arrow).

in this case, namely, that extreme dysfunction which was observed in visuo-spatial memory in the WMS-R visual memory index as well as in the errors on the CDT, which seemed to be inconsequential to the normal MMSE score obtained.

Imaging findings:

Plain X-ray images of hands and fingers revealed multiple bone cysts at the epiphyses (Fig. 1). T2-enhanced brain MRI images revealed diffuse high-intensity areas in the white matter as well as low-intensity areas in the basal ganglia (Fig. 2). FLAIR images showed progressive brain atrophy, with particularly significant bilateral atrophy of the hippocampus. The atrophy of the brain progressed much more rapidly after the patient suffered prolonged convulsive seizures compared to before the seizures.

A statistical analysis of the brain tomographic images obtained via N-isopropyl-p[^{123}I] iodoamphetamine single-photon emission computed tomography (^{123}I-IMP SPECT) was performed (Fig. 3). The spatial distribution of abnormal regional cerebral blood flow (rCBF) was evaluated using the Neurological Statistical Image Analysis Software (3), and the Z score was calculated (11). Data on normal controls aged 30 to 39 years were derived from a normal database (ChibaDB_ver2) developed by Chiba University Hospital for age-group analysis. The result showed a decrease in blood flow to the frontal lobe after the convulsive seizures compared to that before the seizures. Diminished blood flow was also observed in the posterior parietal area, including the precuneus.

Genetic analysis: After informed consent was obtained, high-molecular-weight genomic DNA was extracted from whole peripheral blood using the GenomicPreP blood DNA isolation kit (GE Healthcare UK, Ltd., Buckinghamshire, England). All five exons and 5′ and 3′ flanking regions of the *DAP12* gene (*TYROBP*; GenBank accession No. AF 019563) were amplified by PCR using the primer sets specific for individual exons (3). The purified PCR products

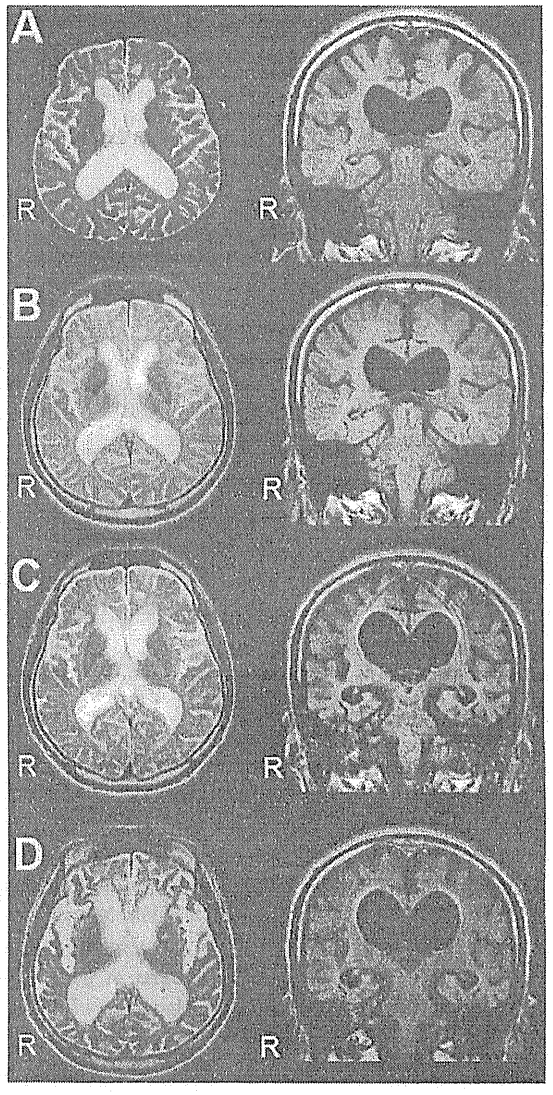

Figure 2. Brain MRI. A, B, C, and D show T2-enhanced images and FLAIR images taken when the patient was 34 and 35 years old, immediately after the onset of convulsive seizures when the patient was 36 years old, and one month after the convulsive seizures, respectively. A comparison of A and B, which represent images taken before the onset of prolonged convulsive seizures, reveals only a mild progression of brain atrophy. In contrast, rapid progression of brain atrophy is evident when comparing C, which represents images taken after the convulsive seizures, and B. D, which represents images taken one month after the convulsive seizures, shows even greater progression of brain atrophy.

were processed for direct sequencing by the dideoxynucleotide chain termination method on the 3730xl DNA Analyzer (Applied Biosystems, Foster City, CA, USA). A single-base deletion of 141 G (141delG) was found in exon 3 of the DAP12 gene (Fig. 4). Furthermore, this genetic mutation was found to be a homozygous point mutation. These findings confirmed the diagnosis of NHD on the basis of a dem-

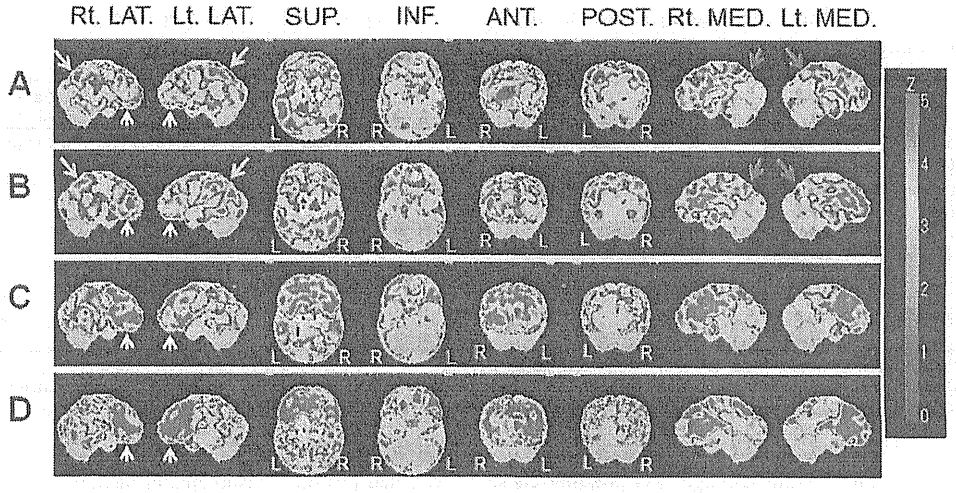

Figure 3. Cerebral blood flow SPECT images. A, B, C, and D show Z-score maps of SPECT images taken when the patient was 34 and 35 years old, after the onset of convulsive seizures when the patient was 36 years old, and one month after the convulsive seizures, respectively. A positive Z score represents a decrease in the regional CBF in the patient relative to the control mean. The red arrows indicate diminished blood flow to the posterior parietal area, including the precuneus. The yellow and white arrows indicate diminished blood flow to the parietal lobe and frontal lobe, respectively. Diminished blood flow to the precuneus, frontal lobe, and parietal lobe was noted even before the onset of convulsive seizures (A, B). After the seizures, however, blood flow to the frontal lobe was markedly diminished (C) and became progressively worse (D). LAT.: lateral, SUP.: superior, INF.: inferior, ANT.: anterior, POST.: posterior, MED.: medial

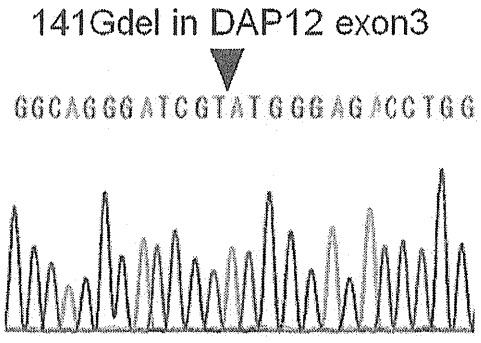

Figure 4. Sequencing analysis of the DAP12 gene. Exons and exon-intron boundaries of the DAP12 gene were amplified from genomic DNA by a polymerase chain reaction (PCR). PCR products were processed for direct sequencing analysis. The figure represents a single-base deletion of 141G (141delG) in exon 3. This genetic mutation was found to be a homozygous point mutation.

onstrated DAP12 gene mutation.

Discussion

The present case is the fifth case of NHD reported in the world with a homozygous mutation (single-base deletion) of 141delG in exon 3 of the DAP12 gene. All reported cases of DAP12 gene mutation (141delG) (3, 6), including the present case, have been Japanese, which suggests that this type of genetic mutation may be specific to the Japanese population.

The clinical characteristics of typical cases of defects in the DAP12 and TREM12 genes reported in the previous studies and the characteristics of the present case are summarized in Table 2 (4, 7). Compared to the previous cases, the present case exhibited an earlier onset of frontal lobe and bone symptoms and a shorter period before the patient became bedridden.

The DAP12 gene mutation (141delG) of the present case involved a frameshift of the open reading frame and the coding of the truncated DAP12 protein with no intracellular tyrosine-based activation motif (ITAM) (8), which can potentially lead to the dysfunction of TREM2/DAP12 signaling cascades. According to the previous reports, TREM2/DAP12 signaling cascades play an important role in immune regulation, including the stimulation of mononuclear phagocytes in the central nervous system (5, 10). Genetic defects lead to the dysfunction of TREM2/DAP12 signaling cascades expressed in the cell membrane of microglia. Under this circumstance, apoptotic nerve cells can no longer be removed by phagocytosis; as a result, the inflammation persists and becomes protracted. These processes are believed to make up the pathological mechanism that underlies the central nervous system damage observed in NHD.

In the present case, rapid progression of brain damage was observed after the onset of prolonged convulsive sei-

Table 2. Comparison of Clinical Symptoms between the Cases Reported Previously and the Case Examined in the Present Study

	Mutation	N (patients)	Age at onset of frontal lobe syndrome (years)	Age at onset of bone pain and fracture (years)	Epileptic seizure	Age at onset of abasia (years)
Paloneva (4) (2001)	DAP12 gene; Del 5.3kb	8	25-40 (mean, 33)	18-33 (mean, 27)	7/8 (87.5 %)	34-47 (mean, 42.5)
Klünemann (7) (2005)	TREM2 gene; 97C > T, 267delG, 313delG, 377T > G	6	22-39 (mean, 33)	21-40 (mean, 31)	ND	ND
Present case	DAP12 gene; 141delG	1	26	18	+	36

ND: Not described

A comparison was made between the clinical characteristics of typical cases of defects in the DAP12 and TREM12 genes reported in previous studies[4,7] and the characteristics of the case reported in the present study

zures. The promotion of brain damage was possibly caused by a failure to phagocytize and delete the apoptotic neurons resulting from the severe epileptic seizures. The control of epileptic seizures is believed to be effective in preventing the progression of brain damage.

The present SPECT findings showed regional cerebral blood flow (rCBF) abnormalities to the cerebral cortex, including the frontal and parietal lobes. These findings were consistent with previously reported results of SPECT and positron emission tomography (PET) images in NHD (7, 12, 13). Unlike the previous reports in which SPECT images were analyzed qualitatively, the present study was designed to identify a statistical image analysis using 3D stereotactic surface projections (3D-SSP). In this way, we were able to examine diminished blood flow to the parietal lobe in a more detailed manner, and we successfully identified diminished blood flow to the posterior parietal area, including the precuneus. The results of the overall psychological tests disclosed the neuropsychological profiles, that is, intact overall cognitive function with memory decline as primary disturbances that resembled MCI (14). SPECT and PET studies of MCI have demonstrated diminished blood flow and metabolism in the posterior cingulate gyrus and precuneus, which are known to have dense fiber connections with medial temporal lesions, such as the hippocampus (15-17). These findings are an important determinant in the diagnosis of MCI, which is believed to be a precursor to Alzheimer's disease. In the present case, the diminished blood flow to the precuneus was also suspected to be the distant effect of hippocampal disorder. On the other hand, the close relationship between the precuneus and spatially guided behaviour is becoming clear (18). The precuneus disorder might be a cause of the memory impairment that is similar to MCI and the characteristic visuo-spatial memory impairment of NHD (19).

NHD is an intractable disease accompanied by symptoms of early-onset dementia. There has been a report of a case of a TREM2 gene mutation in a patient who manifested symptoms of dementia without exhibiting bone lesions (9). Similarly, there have been two reported cases of heterozygous carriers of the mutated allele of TREM2 gene mutation who had profound visuo-spatial memory impairment without exhibiting bone lesions and whose SPECT study revealed the diminished blood flow to the basal ganglia (19). Although NHD is a rare disease, we believe it has important implications in the identification of early-onset dementia accompanied mainly by frontal lobe symptoms.

The authors state that they have no Conflict of Interest (COI).

References

1. Hakola HPA. Neuropsychiatric and genetic aspects of a new hereditary disease characterized by progressive dementia and lipomembranous polycystic osteodysplasia. Acta Psychiatr Scand **232** (suppl): 1-173, 1972.
2. Nasu T, Tsukahara Y, Terayama K. A lipid metabolic disease-"membranous lipodystrophy"-an autopsy case demonstrating numerous peculiar membrane-structures composed of compound lipid in bone and bone marrow and various adipose tissues. Acta Pathol Jpn **23**: 539-558, 1973.
3. Paloneva J, Kestilä M, Wu J, et al. Loss-of-function mutations in TYROBP (DAP12) result in a presenile dementia with bone cysts. Nat Genet **25**: 357-361, 2000.
4. Paloneva J, Autti T, Raininko R, et al. CNS manifestations of Nasu-Hakola disease: a frontal dementia with bone cysts. Neurology **56**: 1552-1558, 2001.
5. Bianchin MM, Capella HM, Chaves DL, et al. Nasu-Hakola disease (polycystic lipomembranous osteodysplasia with sclerosing leukoencephalopathy--PLOSL): a dementia associated with bone cystic lesions. From clinical to genetic and molecular aspects. Cell Mol Neurobiol **24**: 1-24, 2004.
6. Kondo T, Takahashi K, Kohara N, et al. Heterogeneity of presenile dementia with bone cysts (Nasu-Hakola disease): three genetic forms. Neurology **59**: 1105-1107, 2002.
7. Klünemann HH, Ridha BH, Magy L, et al. The genetic causes of basal ganglia calcification, dementia, and bone cysts: DAP12 and TREM2. J. Neurology **64**: 1502-1507, 2005.
8. Kuroda R, Satoh J, Yamamura T, et al. A novel compound heterozygous mutation in the DAP12 gene in a patient with Nasu-Hakola disease. J Neurol Sci **252**: 88-91, 2007.
9. Chouery E, Delague V, Bergougnoux A, Koussa S, Serre JL, Mégarbané A. Mutations in TREM2 lead to pure early-onset dementia without bone cysts. Hum Mutat **29**: E194-E204, 2008.
10. Neumann H, Takahashi K. Essential role of the microglial triggering receptor expressed on myeloid cells-2 (TREM2) for central nervous tissue immune homeostasis. J Neuroimmunol **184**: 92-99,

2007.

11. Minoshima S, Frey KA, Koeppe RA, Foster NL, Kuhl DE. A diagnostic approach in Alzheimer's disease using three-dimensional stereotactic surface projections of fluorine-18-FDG PET. J Nucl Med **36**: 1238-1248, 1995.
12. Ueki Y, Kohara N, Oga T, et al. Membranous lipodystrophy presenting with palilalia: a PET study of cerebral glucose metabolism. Acta Neurol Scand **102**: 60-64, 2000.
13. Takeshita T, Kaminaga T, Tatsumi T, Hatanaka Y, Furui S. Regional cerebral blood flow in a patient with Nasu-Hakola disease. Ann Nucl Med **19**: 309-312, 2005.
14. Petersen RC. Mild cognitive impairment as a diagnostic entity. J Intern Med **256**: 183-194, 2004.
15. Minoshima S, Giordani B, Berent S, Frey KA, Foster NL, Kuhl DE. Metabolic reduction in the posterior cingulate cortex in very early Alzheimer's disease. Ann Neurol **42**: 85-94, 1997.
16. Kogure D, Matsuda H, Ohnishi T, et al. Longitudinal evaluation of early Alzheimer's disease using brain perfusion SPECT. J Nucl Med **41**: 1155-1162, 2000.
17. Chételat G, Desgranges B, de la Sayette V, et al. Dissociating atrophy and hypometabolism impact on episodic memory in mild cognitive impairment. Brain **126**: 1955-1967, 2003.
18. Cavanna A, Trimble MR. The precuneus: a review of its functional anatomy and behavioural correlates. Brain **129**: 564-583, 2006.
19. Montalbetti L, Ratti MT, Greco B, Aprile C, Moglia A, Soragna D. Neuropsychological tests and functional nuclear neuroimaging provide evidence of subclinical impairment in Nasu-Hakola disease heterozygotes. Funct Neurol **20**: 71-75, 2005.